PHYSICAL REVIEW D **76,** 034003 (2007)

Photon-jet correlations in pp and $p\bar{p}$ collisions

T. Pietrycki
Institute of Nuclear Physics, PL-31-342 Cracow, Poland

A. Szczurek
Institute of Nuclear Physics, PL-31-342 Cracow, Poland and University of Rzeszów, PL-35-959 Rzeszów, Poland

(Received 20 April 2007; published 6 August 2007)

We compare results of the k_t-factorization approach and the next-to-leading order collinear-factorization approach for photon-jet correlations in pp and $p\bar{p}$ collisions at Relativistic Heavy Ion Collider, Tevatron, and Large Hadron Collider energies. We discuss correlations in the azimuthal angle as well as in the two-dimensional space of transverse momentum of photon and jet. Different unintegrated parton distributions (UPDF) are included in the k_t-factorization approach. The results depend on UPDFs used. The standard collinear approach gives a cross section comparable to the k_t-factorization approach. For correlations of the photon and any jet the next-to-leading order (NLO) contributions dominate at relatively small azimuthal angles as well as for asymmetric transverse momenta. For correlations of the photon with the leading jet (the one having the biggest transverse momentum) the NLO approach gives zero contribution at $\phi_- < \pi/2$, which opens a possibility to study higher-order terms and/or UPDFs in this region.

DOI: 10.1103/PhysRevD.76.034003 PACS numbers: 12.38.Bx, 13.60.Hb, 13.85.Qk

I. INTRODUCTION

Jet-jet correlations are an interesting probe of QCD dynamics [1]. Recent studies of hadron-hadron correlations at the Relativistic Heavy Ion Collider (RHIC) [2] open a new possibility to study the dynamics of jet and particle production. Hadron-hadron correlations involve both jet-jet correlations as well as complicated jet structure. Recently, preliminary data on photon-hadron azimuthal correlations in nuclear collisions were also presented [3]. In principle, such correlations should be easier for theoretical description as here only one jet enters, at least in leading-order perturbative QCD (pQCD). On the experimental side, such measurements are more difficult due to much reduced statistics as compared to the dijet studies.

Up to now no theoretical calculation for photon-jet was presented in the literature, even for elementary collisions. In the leading-order collinear-factorization approach the photon and the associated jet are produced back-to-back. If transverse momenta of partons entering the hard process are included, the transverse momenta of the photon and the jet are no longer balanced and finite (nonzero) correlations in a broad range of relative azimuthal angle and/or in lengths of transverse momenta of the photon and the jet are obtained. The finite correlations can be also obtained in higher orders of the collinear-factorization approach [4]. To our knowledge, no detailed studies for present accelerators have been presented in the literature.

In contrast to the coincidence studies the inclusive distributions of photons were studied carefully in pQCD up to the next-to-leading order [5]. Similar studies were performed recently also in the k_t-factorization approach [6,7]. A rather good description of direct-photon inclusive cross sections can be obtained in both approaches. The k_t-factorization approach offers a relatively easy method to calculate photon-jet correlations [7].

The k_t-factorization approach was used recently to several high-energy reactions, including heavy quark pair photo- [8,9] and hadroproduction [10,11], charmonium production [12,13], inclusive Z^0 [14], and Higgs [15,16] production.

In the present paper we shall compare results obtained in the leading-order k_t-factorization approach and the next-to-leading-order collinear-factorization approach. We shall discuss which approach is more adequate for different regions of phase space. We shall present corresponding results for proton-proton scattering at RHIC and LHC and proton-antiproton scattering at Tevatron.

II. FORMALISM

A. $2 \to 2$ contributions with unintegrated parton distributions

In Fig. 1 we show a complete set of diagrams that appear in the k_t-factorization approach to photon-jet correlations. It is known that at midrapidities and at relatively small transverse momenta, photon-jet production is dominated by (sub)processes initiated by gluons.

In the k_t-factorization approach, the cross section for simultaneous production of a photon and an associated jet in the collisions of two hadrons (pp or $p\bar{p}$) can be written as

$$\frac{d\sigma_{h_1 h_2 \to \gamma k}}{d^2 p_{1,t} d^2 p_{2,t}} = \int dy_1 dy_2 \frac{d^2 k_{1,t}}{\pi} \frac{d^2 k_{1,t}}{\pi} \frac{1}{16\pi^2 (x_1 x_2 s)^2} \times \overline{|\mathcal{M}_{ij\to\gamma k}|^2} \delta^2(\vec{k}_{1,t} + \vec{k}_{2,t} - \vec{p}_{1,t} - \vec{p}_{2,t}) \times \mathcal{F}_i(x_1, k_{1,t}^2, \mu_1^2) \mathcal{F}_j(x_2, k_{2,t}^2, \mu_2^2), \quad (1)$$

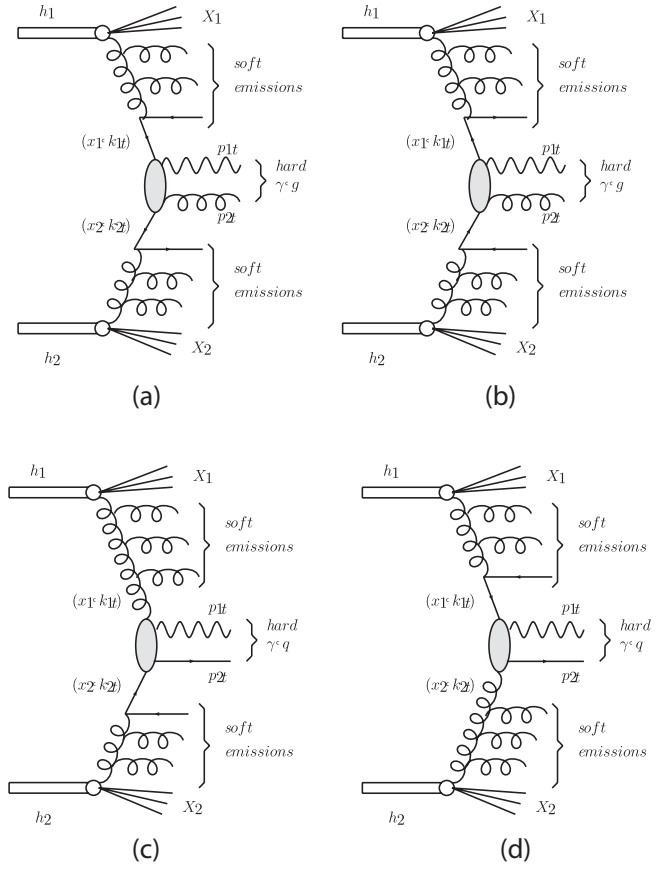

FIG. 1. Basic diagrams of the k_t-factorization approach to photon-jet correlations.

where $\mathcal{F}_i(x_1, k_{1,t}^2, \mu_1^2)$ and $\mathcal{F}_j(x_2, k_{2,t}^2, \mu_2^2)$ are so-called unintegrated parton distributions. Longitudinal momentum fractions are evaluated as

$$x_1 = (m_{1t}e^{+y_1} + m_{2t}e^{+y_2})/\sqrt{s},$$
$$x_2 = (m_{1t}e^{-y_1} + m_{2t}e^{-y_2})/\sqrt{s}. \tag{2}$$

We shall return to the choice of the factorization scale in the next section. Its role is completely different in different approaches, i.e., different choices of UPDFs. Special attention will be devoted to the Kwieciński UPDF and the role of the scale parameter there.

If one makes the following replacement

$$\mathcal{F}_i(x_1, k_{1,t}^2, \mu_1^2) \to x_1 p_i(x_1, \mu_1^2)\delta(k_{1,t}^2),$$
$$\mathcal{F}_j(x_2, k_{2,t}^2, \mu_2^2) \to x_2 p_j(x_2, \mu_2^2)\delta(k_{2,t}^2) \tag{3}$$

and

$$\mathcal{M}_{ij\to\gamma k}(k_{1,t}^2, k_{2,t}^2) \to \mathcal{M}_{ij\to\gamma k}(k_{1,t}^2 = 0, k_{2,t}^2 = 0) \tag{4}$$

then one recovers the standard leading-order collinear formula.

The final partonic state is $\gamma k = \gamma g, \gamma q$. Matrix elements for corresponding processes are discussed in the appendix. As explained in the appendix, our matrix elements are obtained as extrapolation of standard on-shell matrix elements to off-shell kinematics. We have also used exact matrix elements obtained in Ref. [6], which include longitudinal photons. In the limit $k_{1,t} \to 0$ and $k_{2,t} \to 0$ one reproduces the familiar on-shell matrix element.

The inclusive invariant cross section for direct-photon production can be written as

$$\frac{d\sigma_{h_1h_2\to\gamma}}{dy_1 d^2p_{1,t}} = \int dy_2 \frac{d^2k_{1,t}}{\pi}\frac{d^2k_{2,t}}{\pi}(\ldots)|_{\vec{p}_{2,t}=\vec{k}_{1,t}+\vec{k}_{2,t}-\vec{p}_{1,t}} \tag{5}$$

and analogously the cross section for the associated parton (jet) can be written as

$$\frac{d\sigma_{h_1h_2\to k}}{dy_1 d^2p_{1,t}} = \int dy_1 \frac{d^2k_{1,t}}{\pi}\frac{d^2k_{2,t}}{\pi}(\ldots)|_{\vec{p}_{1,t}=\vec{k}_{1,t}+\vec{k}_{2,t}-\vec{p}_{2,t}}. \tag{6}$$

Let us return to the coincidence cross section. The integration with the Dirac delta function in Eq. (1)

$$\int dy_1 dy_2 \frac{d^2k_{1,t}}{\pi}\frac{d^2k_{2,t}}{\pi}(\ldots)\delta^2(\ldots) \tag{7}$$

can be performed by introducing the following new auxiliary variables:

$$\vec{Q}_t = \vec{k}_{1,t} + \vec{k}_{2,t}, \qquad \vec{q}_t = \vec{k}_{1,t} - \vec{k}_{2,t}. \tag{8}$$

Then our initial cross section can be written as

$$\frac{d\sigma_{h_1h_2\to\gamma,\text{parton}}}{d^2p_{1,t}d^2p_{2,t}} = \frac{1}{4}\int dy_1 dy_2 \frac{1}{2} dq_t^2 d\phi_{q_t}(\ldots)|_{\vec{Q}_t=\vec{P}_t}. \tag{9}$$

Above $\vec{P}_t = \vec{p}_{1,t} + \vec{p}_{2,t}$. The factor $\frac{1}{4}$ in front of the integral on the right-hand side of Eq. (9) comes from the Jacobian of the $(\vec{k}_{1,t}, \vec{k}_{2,t}) \to (\vec{Q}_t, \vec{q}_t)$ transformation (see [7]).

B. 2 → 3 contributions in NLO collinear-factorization approach

Up to now we have concentrated only on processes with two explicit hard partons (γk) in the k_t-factorization approach. It is of interest to compare the results of our approach with those of the standard collinear next-to-leading-order approach. In this section we discuss processes with three explicit hard partons. In Fig. 2 we show diagrams for $2 \to 3$ subprocesses included in our calculations. In the following we assume particle No. 1 to be a photon. Then particle No. 2 is g, q, and $\bar{q}$, depending on the subprocess.

The cross section for $h_1h_2 \to \gamma klX$ processes can be calculated according to the standard parton model formula

$$d\sigma_{h_1h_2\to\gamma kl} = \sum_{ijk}\int dx_1 dx_2 p_i(x_1, \mu^2) p_j(x_2, \mu^2) d\hat{\sigma}_{ij\to\gamma kl}. \tag{10}$$

The elementary cross section can be written as

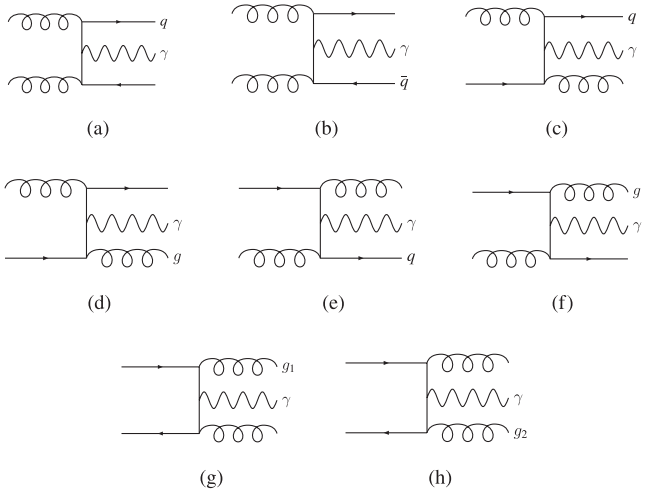

FIG. 2. Diagrams for NLO collinear-factorization approach for photon-jet-jet production.

$$d\hat{\sigma}_{ij\to\gamma kl} = \frac{1}{2\hat{s}}\overline{|\mathcal{M}_{ij\to\gamma kl}|^2}dR_3, \tag{11}$$

where the three-body phase space element reads

$$dR_3 = (2\pi)^4\delta^4\Big(p_a + p_b - \sum_{i=1}^{3} p_i\Big)\prod_{i=1}^{3}\frac{d^3p_i}{2E_i(2\pi)^3}. \tag{12}$$

This element can be expressed in an equivalent way in terms of parton rapidities

$$dR_3 = (2\pi)^4\delta^4\Big(p_a + p_b - \sum_{i=1}^{3} p_i\Big)\prod_{i=1}^{3}\frac{dy_i d^2p_{i,t}}{(4\pi)(2\pi)^2}. \tag{13}$$

The last formula is useful for practical applications. Now the cross section for hadronic collisions can be written in terms of the $2 \to 3$ matrix element as

$$d\sigma = \sum_{ijkl} dy_1 d^2p_{1,t} dy_2 d^2p_{2,t} dy_3 \frac{1}{(4\pi)^3(2\pi)^2} \times \frac{1}{\hat{s}^2} x_1 p_i(x_1, \mu^2) x_2 p_j(x_2, \mu^2)\overline{|\mathcal{M}_{ij\to\gamma kl}|^2}, \tag{14}$$

where the longitudinal momentum fractions are evaluated as

$$x_1 = \frac{1}{\sqrt{s}}\sum_{i=1}^{3} p_{i,t}e^{+y_i}, \qquad x_2 = \frac{1}{\sqrt{s}}\sum_{i=1}^{3} p_{i,t}e^{-y_i}. \tag{15}$$

Repeating similar steps as for $2 \to 2$ processes we get finally

$$d\sigma = \sum_{ijkl}\frac{1}{64\pi^4\hat{s}^2} x_1 p_i(x_1, \mu^2) x_2 p_j(x_2, \mu^2)\overline{|\mathcal{M}_{ij\to\gamma kl}|^2} \times p_{1,t}dp_{1,t}p_{2,t}dp_{2,t}d\phi_- dy_1 dy_2 dy_3, \tag{16}$$

where the relative azimuthal angle between the photon and the associated jet (ϕ_-) is restricted to the interval $(0, \pi)$. The last formula is very useful in calculating the cross section for particle 1 and particle 2 correlations.

III. RESULTS

In this section we shall present results for RHIC and Tevatron energies. We use UPDFs from the literature. There are only two complete sets of UPDFs in the literature which include not only the gluon distributions but also the distributions of quarks and antiquarks:

(a) Kwieciński [17],
(b) Kimber-Martin-Ryskin [18].

For comparison we shall include also the unintegrated parton distributions obtained from the collinear ones by the Gaussian smearing procedure. Such a procedure is often used in the context of direct photons [19,20]. Comparing results obtained with those Gaussian distributions and the results obtained with the Kwieciński distributions with nonperturbative Gaussian form factors will allow one to quantify the effect of UPDF evolution as contained in the Kwieciński evolution equations. What is the hard scale for our process? In our case the best candidate for the scale is the photon and/or jet transverse momentum squared. Since we are interested in rather small transverse momenta the evolution length is not too large and the deviations from initial k_t distributions (assumed here to be Gaussian) should not be too big.

At high energies one enters into a small-x region, i.e., the region of a specific dynamics of the QCD emissions. In this region only unintegrated distributions of gluons exist in the literature. In our case the dominant contributions come from QCD-Compton gluon-quark or quark-gluon initiated hard subprocesses. This means that we need unintegrated distributions of both gluons and quarks/antiquarks. In this case we take such UGDFs from the literature and supplement them by the Gaussian distributions of quarks/antiquarks.

Let us start from presenting our results on the $(p_{1,t}, p_{2,t})$ plane. In Fig. 3 we show the maps for different UPDFs used in the k_t-factorization approach as well as for NLO collinear-factorization approach for $p_{1,t}, p_{2,t} \in (5, 20)$ GeV and at the Tevatron energy $W = 1960$ GeV. In the case of the Kwieciński distribution we have taken $b_0 = 1\ \mathrm{GeV}^{-1}$ for the exponential nonperturbative form factor and the scale parameter $\mu^2 = 100\ \mathrm{GeV}^2$. Rather similar distributions are obtained for different UPDFs. The distribution obtained in the NLO approach differs qualitatively from those obtained in the k_t-factorization approach. First of all, one can see a sharp ridge along the diagonal $p_{1,t} = p_{2,t}$. This ridge corresponds to a soft singularity when the unobserved parton has very small transverse momentum $p_{3,t}$. As will be clear in a moment this corresponds to the azimuthal angle between the photon and the jet being $\phi_- = \pi$. Obviously this is a region that cannot be reliably calculated in collinear pQCD. There are different practical possibilities to exclude this region from the calculations. The most primitive way (possible only in theoretical calculations) is to impose a lower cut on transverse momentum of the unobserved parton $p_{3,t}$.

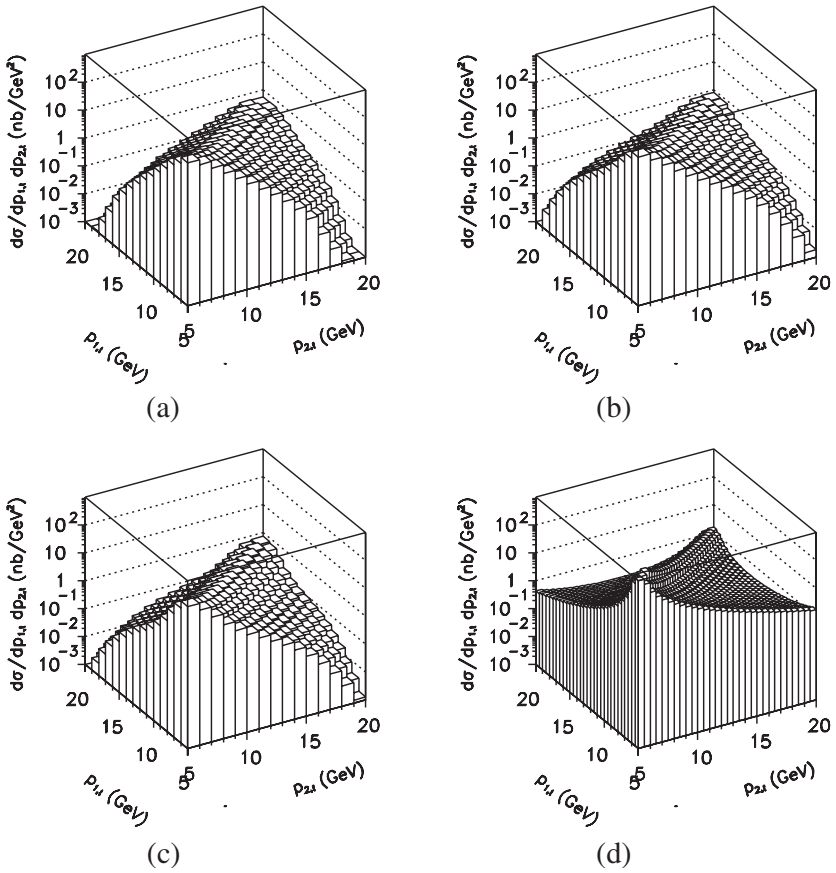

FIG. 3. Transverse-momentum distributions $d\sigma/dp_{1,t}dp_{2,t}$ at $W = 1960$ GeV and for different UPDFs in the k_t-factorization approach for Kwieciński ($b_0 = 1$ GeV^{-1}, $\mu^2 = 100$ GeV^2) (a), BFKL (b), KL (c), and NLO $2 \to 3$ collinear-factorization approach including diagrams from Fig. 2(d). The integration over rapidities from the interval $-5 < y_1, y_2 < 5$ is performed.

Second, the standard collinear NLO approach generates a much bigger cross section at configurations asymmetric in $p_{1,t}$ and $p_{2,t}$. We shall return to this observation in the course of this paper.

As discussed in Ref. [7], Kwieciński distributions are very useful to treat both the nonperturbative (intrinsic nonperturbative transverse momenta) and the perturbative (QCD broadening due to parton emission) effects on the

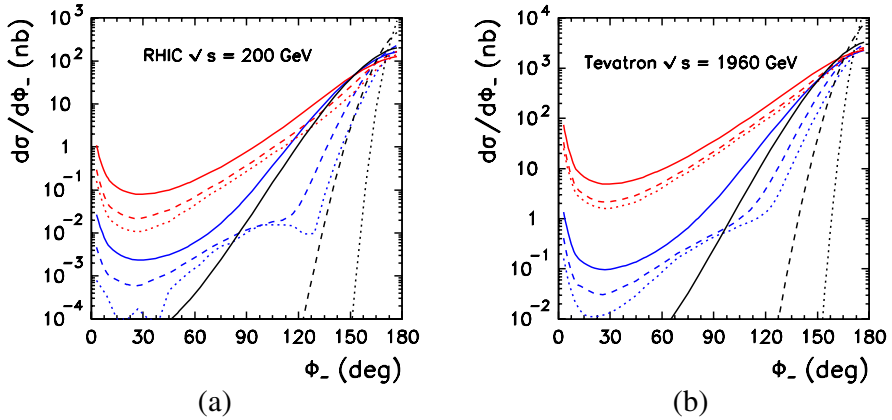

FIG. 4 (color online). Azimuthal angle correlation functions at (a) RHIC, (b) Tevatron energies for different scales and different values of b_0 of the Kwieciński distributions. The solid line is for $b_0 = 0.5$ GeV^{-1}, the dashed line is for $b_0 = 1$ GeV^{-1}, and the dotted line is for $b_0 = 2$ GeV^{-1}. Three different values of the scale parameters are shown: $\mu^2 = 0.25, 10, 100$ GeV^2 [the bigger the scale the bigger the decorrelation effect, different colors (shades) on line]. In this calculation $p_{1,t}, p_{2,t} \in (5, 20)$ GeV and $y_1, y_2 \in (-5, 5)$.

same footing. In Fig. 4 we show the effect of the scale evolution of the Kwieciński UPDFs on the azimuthal angle correlations between the photon and the associated jet. We show results for different initial conditions ($b_0 = 0.5$, 1.0, 2.0 GeV^{-1}). At the initial scale (fixed here as in the original GRV [21] to be $\mu^2 = 0.25$ GeV^2) there is a sizeable difference of the results for different b_0. The difference becomes less and less pronounced when the scale increases. At $\mu^2 = 100$ GeV^2 the differences practically disappear. This is due to the fact that the QCD-evolution broadening of the initial parton transverse-momentum distribution is much bigger than the typical initial nonperturbative transverse-momentum scale.

In Fig. 5 we show corresponding azimuthal angular correlations for three different energies relevant for RHIC, Tevatron, and LHC. In this case integration is made over transverse momenta $p_{1,t}$, $p_{2,t} \in (5, 20)$ GeV and rapidities y_1, $y_2 \in (-5, 5)$. The standard NLO collinear cross section grows somewhat faster with energy than the k_t result with unintegrated Kwieciński distribution. This is partially due to an approximation made in the calculation of off-shell matrix elements. Up to now we have used matrix elements called "on-shell" (for an explanation, see the appendix). This approximation is expected to be reliable for small transverse momenta of initial gluons (for a detailed discussion, see Ref. [7]). For larger gluon transverse momenta the longitudinal gluons start to play an important role. This is obviously not included in our simple extrapolation of the on-shell formula.

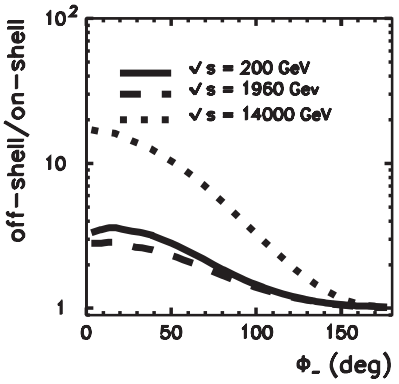

FIG. 6. Off-shell to so-called on-shell cross section ratio as a function of relative azimuthal angle for proton-(anti)proton collision at $W = 200$ GeV (solid), $W = 1960$ GeV (dashed), $W = 14\,000$ GeV for the Kwieciński UPDFs within the k_t-factorization approach. Here y_1, $y_2 \in (-5, 5)$.

In Fig. 6 we show the ratio of the cross section obtained with the two approaches. While at relative azimuthal angles close to π the two approaches coincide, they start to

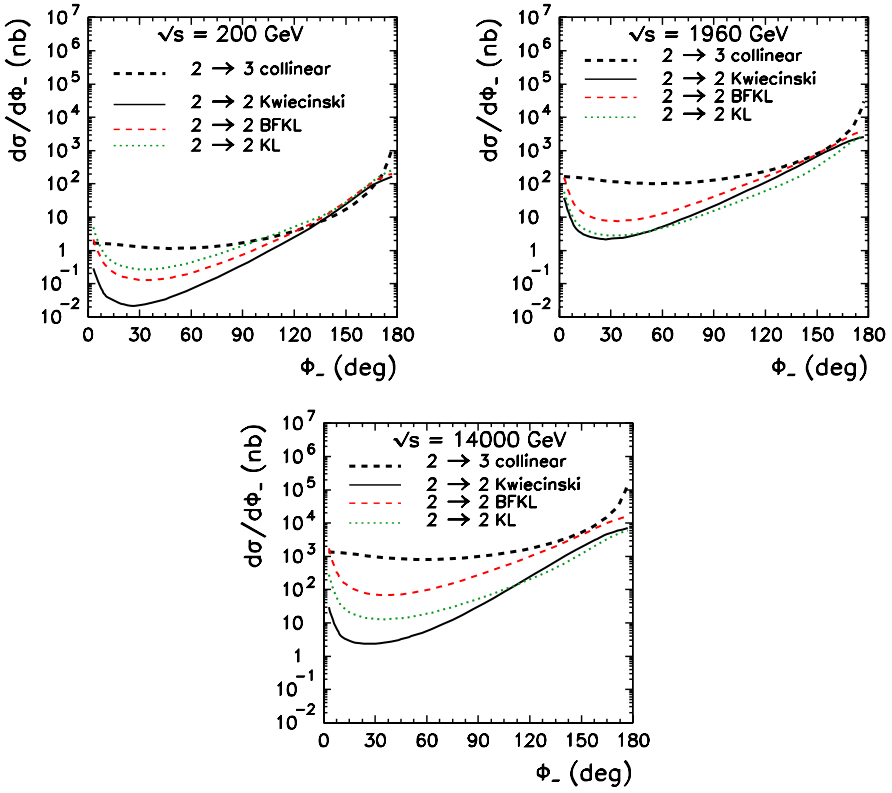

FIG. 5 (color online). Photon-jet angular azimuthal correlations $d\sigma/d\phi_-$ for proton-(anti)proton collision at $W = 200$, 1960, 14 000 GeV for different UPDFs in the k_t-factorization approach for the Kwieciński (solid), BFKL (dashed), KL (dotted) UPDFs/UGDFs, and for the NLO collinear-factorization approach (thick dashed). Here y_1, $y_2 \in (-5, 5)$.

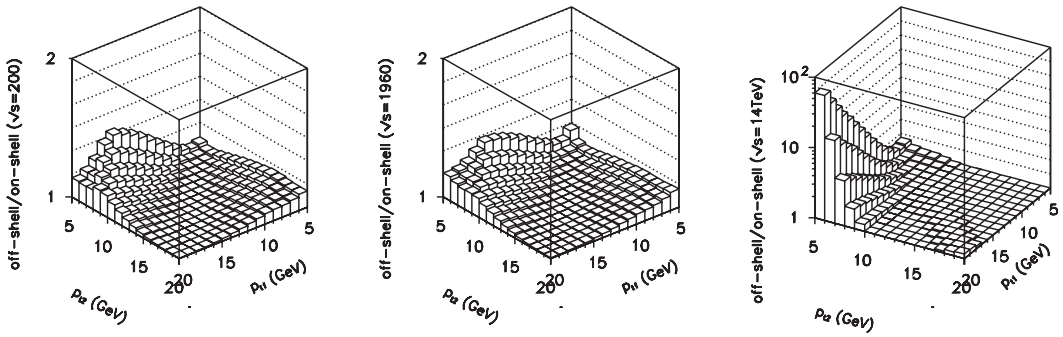

FIG. 7. Off-shell to so-called on-shell cross section ratio as a function of transverse momentum of the photon and jet at $W = 200$ GeV (a), $W = 1960$ GeV (b), $W = 14\,000$ GeV (c) for the Kwieciński UPDF ($b_0 = 1$ GeV^{-1}, $\mu^2 = 100$ GeV^2). The integration over rapidities from the interval $-5 < y_1, y_2 < 5$ is performed.

diverge when approaching $\pi = 0$. This can be understood as follows. In the k_t $2 \to 2$ approach the emission of the photon and jet at the same azimuthal angle ($\phi \sim 0$) must necessarily involve large ''initial'' transverse momenta, where deviations from the simple extrapolation can be expected. This means that the azimuthal angular distributions in this region should be calculated rather from the exact formula. The larger the energy the worse the result obtained by extrapolating the matrix element.

In Fig. 7 we show the same ratio as a function of transverse momentum of the photon and jet. Far from the diagonal we observe large deviations from the approximate result. Of course, by definition this is the region of large initial gluon transverse momenta where longitudinal gluons become important.

The singularity in NLO pQCD at $\phi_- = \pi$ is strongly correlated with the sharp ridge in Fig. 3(d). This is demonstrated in Fig. 8 where we present the results of azimuthal correlation function obtained for different cuts on $p_{3,t}$. The cut modifies only the region of relative azimuthal angles close to π. Such a cut would remove also the singularity along the diagonal $p_{1,t} = p_{2,t}$ present in Fig. 3(d) and called here a ridge for easy reference. We

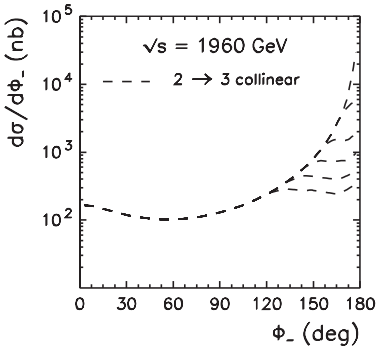

FIG. 8. Photon-jet angular azimuthal correlations $d\sigma/d\phi_-$ for proton-antiproton collision at $W = 1960$ GeV for the NLO collinear-factorization approach and different cuts on $p_{3,t}$. Here $y_1, y_2 \in (-5, 5)$.

wish to stress in this context that there are no singularities of the ridge type in the k_t-factorization approach.

These are small transverse momenta of the unobserved jet which contribute to the sharp ridge along the diagonal $p_{1,t} = p_{2,t}$. It is therefore difficult to distinguish these three-parton states from the states with two partons. The ridge can be eliminated in calculation by imposing a cut on the transverse momentum of the third (unobserved) parton. In experiments there is no possibility to impose such cuts and other methods must be used. We shall return to this point later in this paper.

In Fig. 9 we show angular azimuthal correlations for different interrelations between transverse momenta of outgoing photon and partons: (a) with no constraints on $p_{3,t}$, (b) the case where the $p_{2,t} > p_{3,t}$ condition (called the leading-jet condition in the following) is imposed, (c) $p_{2,t} > p_{3,t}$, and an additional condition $p_{1,t} > p_{3,t}$. The results depend significantly on the scenario chosen as can be seen from the figure. The general pattern is very much the same for different energies.

In Fig. 10 we show two-dimensional transverse-momentum distribution $d\sigma/dp_{1,t}dp_{2,t}(p_{1,t}, p_{2,t})$ for the same extra conditions imposed before in Fig. 9 for azimuthal angle correlations. Imposing the condition that the associated jet is the leading jet ($p_{2,t} > p_{3,t}$) causes the large part of the phase space $p_{1,t} < 2p_{2,t}$ to not be available in the next-to-leading approach. If one imposes in addition that $p_{1,t}$(photon) $> p_{3,t}$(unobserved jet) then also the $p_{2,t} < 2p_{1,t}$ region becomes excluded for the NLO approach. These NLO-excluded regions are therefore regions sensitive to higher-order corrections in pQCD.

In general, the correlations between the photon and the jet depend strongly on all kinematical variables—transverse momenta, azimuthal angles, etc. In order to expose this better, in Fig. 11 we define windows in the $(p_{1,t}, p_{2,t})$ plane which will be used in the following to study azimuthal correlations. At lower energies (as for RHIC) a region of rather low transverse momenta is more adequate (left figure). At larger energies (as for Tevatron) also a region of somewhat larger transverse momenta can be of interest

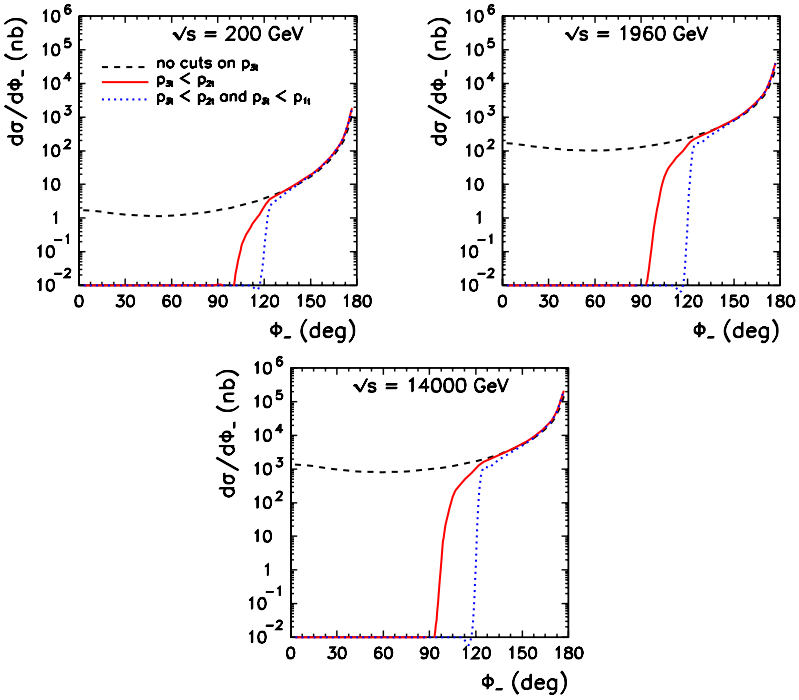

FIG. 9 (color online). Angular azimuthal correlations for different cuts on the transverse momentum of third (unobserved) parton in the NLO collinear-factorization approach without any extra constraints (dashed), $p_{3,t} < p_{2,t}$ (solid), $p_{3,t} < p_{2,t}$ and $p_{3,t} < p_{1,t}$ in addition (dotted). Here $W = 200$, 1960, 14 000 GeV, and y_1, $y_2 \in (-5, 5)$.

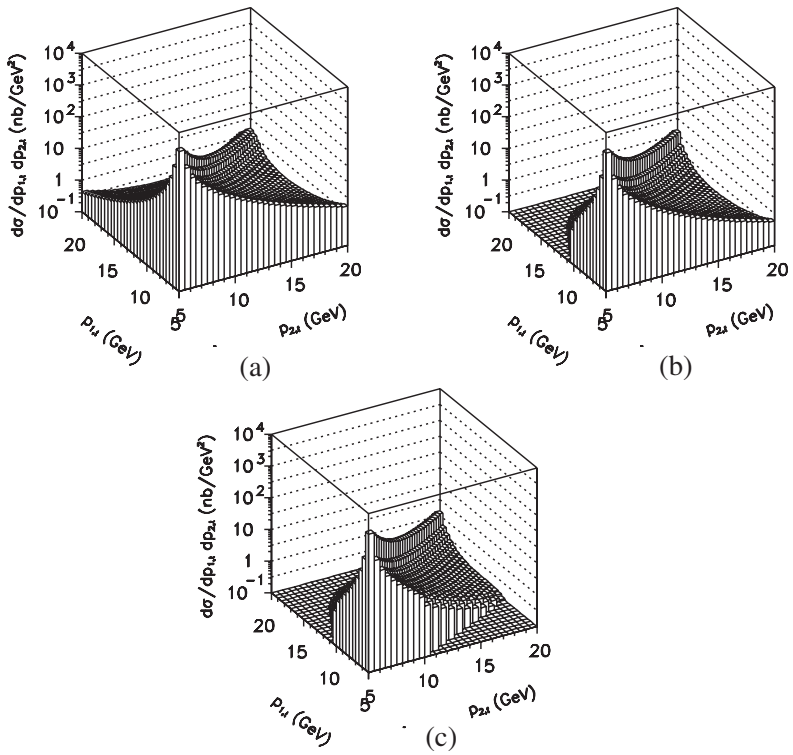

FIG. 10. Two-dimensional distributions in transverse momenta of the photon and jet ($W = 1960$ GeV) $d\sigma/dp_{1,t}dp_{2,t}$ for different constraints on the transverse momentum of third (unobserved) parton in the NLO collinear-factorization approach with no constraints on $p_{3,t}$ (a), $p_{3,t} < p_{2,t}$ (b), $p_{3,t} < p_{2,t}$ and $p_{3,t} < p_{1,t}$ (c). All $2 \to 3$ processes shown in Fig. 2 were included. Here y_1, $y_2 \in (-5, 5)$.

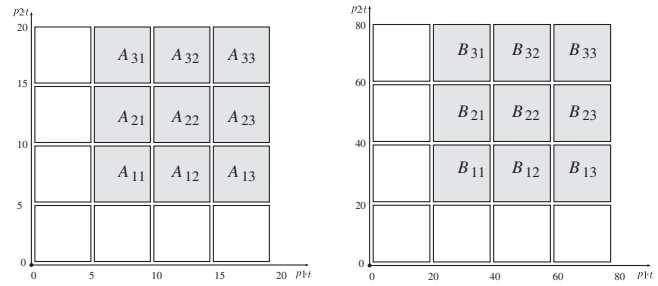

FIG. 11. The definition of the windows in $(p_{1,t}, p_{2,t})$ plane for RHIC energy $\sqrt{s} = 200$ GeV (a) and for Tevatron energy $\sqrt{s} = 1960$ GeV (b).

(right figure). The notation shown in the figure will be used for brevity in the rest of this paper for easy reference.

In Fig. 12 we show angular azimuthal correlations $d\sigma/d\phi_-$ at RHIC energy $\sqrt{s} = 200$ GeV for the Kwieciński UPDFs in the k_t-factorization approach with on-shell (extrapolation method) and off-shell matrix elements and for the NLO collinear-factorization approach with extra leading-jet condition $p_{3,t} < p_{2,t}$. Here the transverse momentum of the photon $(p_{1,t})$ and that of the associated jet $(p_{2,t})$ belong to the interval (5, 20) GeV. For the RHIC energy there is almost no difference between results obtained with off-shell and on-shell (see appendix) matrix elements.

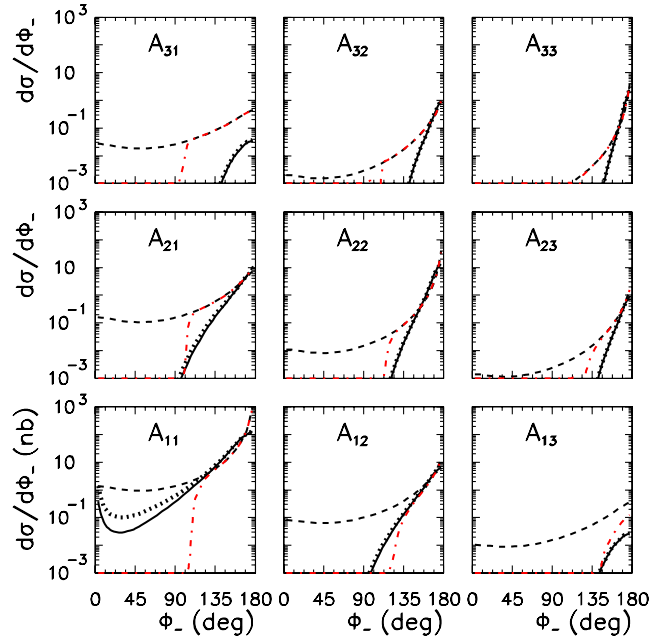

FIG. 12 (color online). Angular azimuthal correlations $d\sigma/d\phi_-$ at $\sqrt{s} = 200$ GeV for Kwieciński UPDFs and on-shell ME (solid), Kwieciński UPDFs and off-shell ME (thick dotted), NLO collinear with no cuts on $p_{3,t}$ (dashed), and NLO collinear with cut on $p_{3,t} < p_{2,t}$ (dash-dotted). Here y_1, $y_2 \in (-5, 5)$.

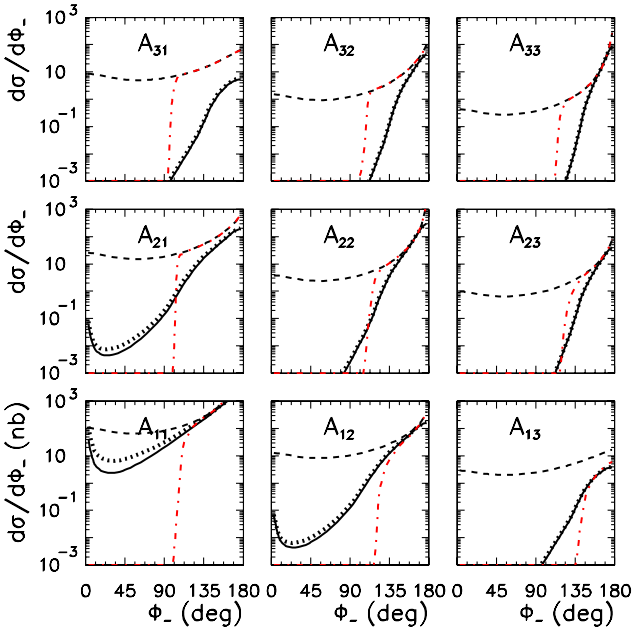

FIG. 13 (color online). Angular azimuthal correlations $d\sigma/d\phi_-$ at $\sqrt{s} = 1960$ GeV for Kwieciński UPDFs and on-shell ME (solid), Kwieciński UPDFs and off-shell ME (thick dotted), NLO collinear with no cuts on $p_{3,t}$ (dashed), and NLO collinear with cut on $p_{3,t} < p_{2,t}$ (dash-dotted). Here y_1, $y_2 \in (-5, 5)$.

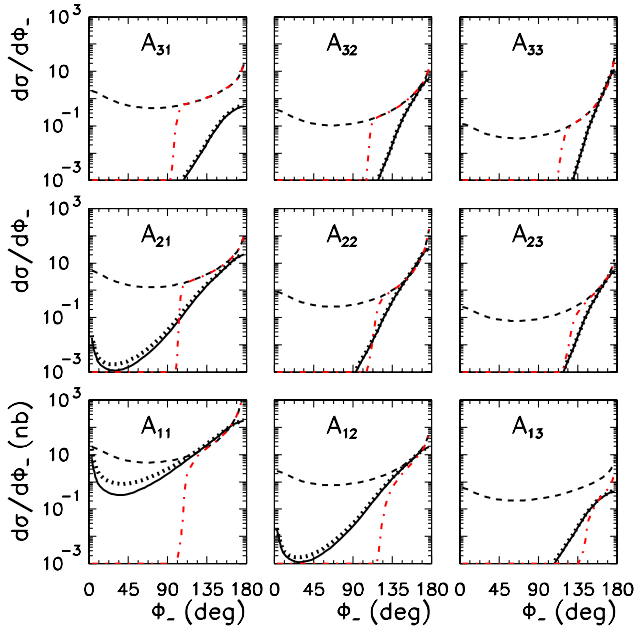

FIG. 14 (color online). Angular azimuthal correlations $d\sigma/d\phi_-$ at $\sqrt{s} = 1960$ GeV for Kwieciński UPDFs and on-shell ME (solid), Kwieciński UPDFs and off-shell ME (thick dotted), NLO collinear with no cuts on $p_{3,t}$ (dashed) and NLO collinear with cut on $p_{3,t} < p_{2,t}$ (dash-dotted). Here $|y_1|$, $|y_2| < 0.9$.

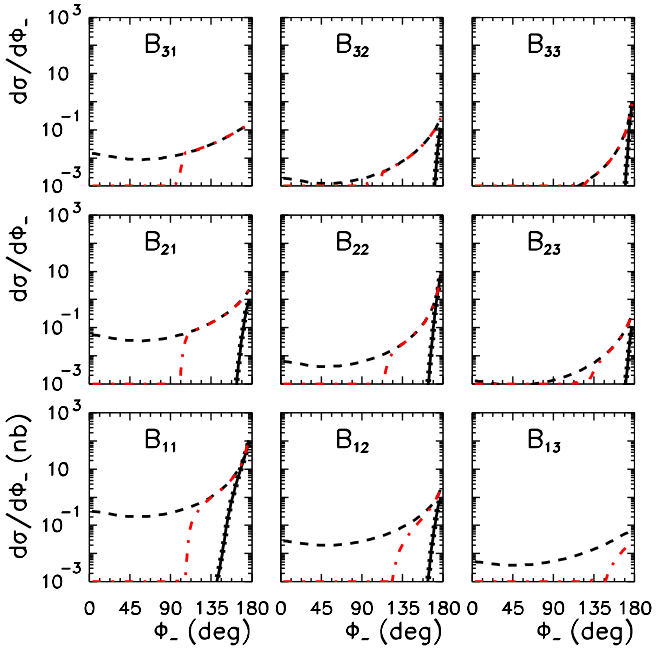

FIG. 15 (color online). Angular azimuthal correlations $d\sigma/d\phi_-$ at $\sqrt{s} = 1960$ GeV for Kwieciński UPDFs and on-shell ME (solid), Kwieciński UPDFs and off-shell ME (thick-dotted) NLO collinear with no cuts on $p_{3,t}$ (dashed) and, NLO collinear with cut on $p_{3,t} < p_{2,t}$ (dash-dotted). Here y_1, $y_2 \in (-5, 5)$.

In Fig. 13 we show analogous angular distributions as in Fig. 12 but for Tevatron energy $\sqrt{s} = 1960$ GeV. In Fig. 14 we show angular correlations for a restricted range of rapidities $|y_1|$, $|y_2| < 0.9$ (corresponding to the present Tevatron apparatus) of the photon and the correlated jet. Limiting to midrapidities does not change the shape of azimuthal correlations significantly.

In Fig. 15 we show similar distributions as in Fig. 13 but for transverse-momentum windows spanned over a broader range of transverse momenta $p_{1,t}$, $p_{2,t} \in (20, 80)$ GeV for the photon and the jet. We observe a slightly faster decrease of the k_t-factorization cross sections for larger $p_{1,t}$ and $p_{2,t}$.

The standard collinear approach can be applied only in the region that is free of singularities. In order to eliminate the regions where the pQCD calculation is not reliable some cuts on the measured transverse momenta must be applied. The simplest method is to use cuts shown in Fig. 16. Mathematically this means that $p_{1,t} > p_{\rm cut}$, $p_{2,t} > p_{\rm cut}$, and

$$|p_{1,t} - p_{2,t}| > \Delta_S. \tag{17}$$

We shall call the last cut a scalar cut for further easy reference. In Fig. 17 we show the azimuthal angle correlation function for different values of the scalar cut $\Delta_S = 0, 1, 2, 3$ GeV. Clearly the NLO singularity at $\phi_- = \pi$ can

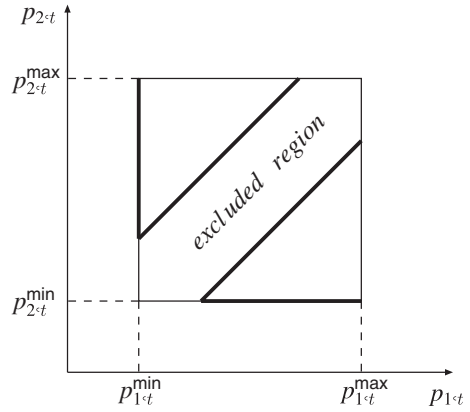

FIG. 16. Diagram showing excluded region in $(p_{1,t}, p_{2,t})$ plane.

be removed by imposing the cut. However, the cut lowers also the k_t-factorization cross section.

We have also tried another option to cut off the singularity:

$$|\vec{p}_{1,t} + \vec{p}_{2,t}| > \Delta_V. \tag{18}$$

This type of the cut we call here vector one for brevity. In Fig. 18 we show a corresponding photon-jet azimuthal angle correlation function with different values of the cut $\Delta_V = 0, 1, 2, 3$ GeV. The situation here is very similar to that for the scalar cut.

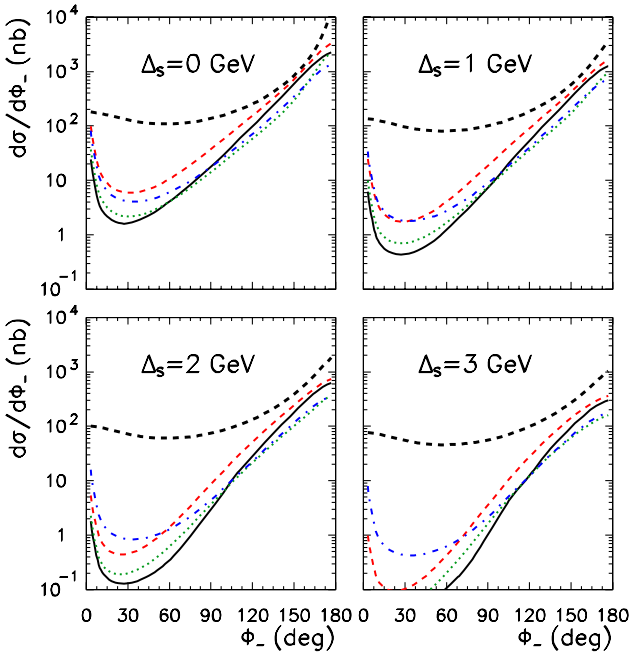

FIG. 17 (color online). Angular azimuthal correlations $d\sigma/d\phi_-$ at $\sqrt{s} = 1960$ GeV for different (scalar) cuts $\Delta_S = 0, 1, 2, 3$ GeV for NLO collinear (dashed), Kwieciński (solid), BFKL (dashed), KL (dotted), and KMR (dash-dotted). Here $p_{1,t}$, $p_{2,t} \in (5, 20)$ GeV and y_1, $y_2 \in (-5, 5)$.

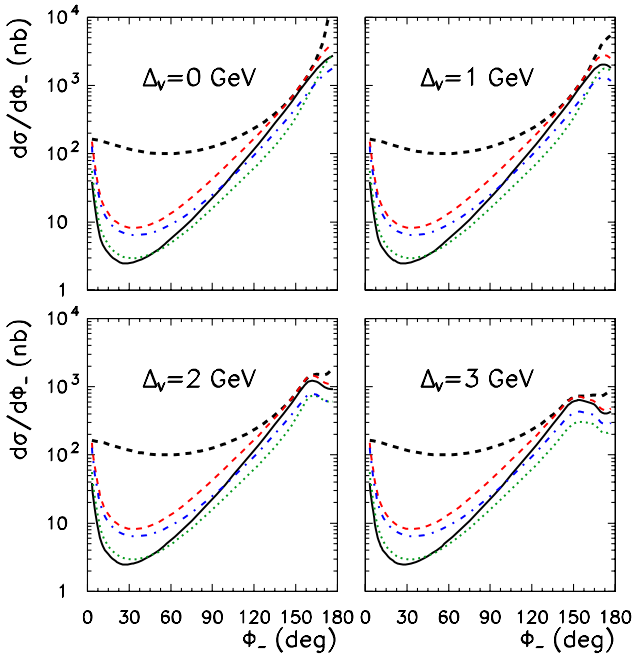

FIG. 18 (color online). Angular azimuthal correlations $d\sigma/d\phi_-$ at $\sqrt{s} = 1960$ GeV for different (vector) cuts $\Delta_V = 0, 1, 2, 3$ GeV for NLO collinear (dashed), Kwieciński (solid), BFKL (dashed), KL (dotted), and KMR (dash-dotted). Here $p_{1,t}$, $p_{2,t} \in (5, 20)$ GeV and $y_1, y_2 \in (-5, 5)$.

IV. CONCLUSIONS

We have performed for the first time the calculation of the photon-jet correlation observables in proton-proton (RHIC, LHC) and proton-antiproton (Tevatron) collisions—a calculation that is lacking in the literature. Up to now such correlations have not been studied experimentally either. We have concentrated on the region of small transverse momenta (semihard region) where the k_t-factorization approach seems to be the most efficient and theoretically justified tool. We have calculated correlation observables for different unintegrated parton distributions from the literature. Our previous analysis of inclusive spectra of direct photons suggests that the Kwieciński distributions give the best description at low and intermediate energies. We have discussed the role of the evolution scale of the Kwieciński UPDFs on the azimuthal correlations. In general, the bigger the scale the bigger decorrelation in azimuth is observed. When the scale $\mu^2 \sim p_t^2(\text{photon}) \sim p_t^2(\text{associated jet})$ (for the kinematics chosen $\mu^2 \sim 100$ GeV^2) is assumed, much bigger decorrelations can be observed than from the standard Gaussian smearing prescription often used in phenomenological studies.

The correlation function depends strongly on whether it is the correlation of the photon and any jet or the correlation of the photon and the leading jet which is considered. In the last case there are regions in azimuth and/or in the two-dimensional $(p_{1,t}, p_{2,t})$ space that cannot be populated in the standard next-to-leading-order approach. In the latter case, k_t factorization seems to be a useful and efficient tool.

We believe that photon-jet correlations can be measured at Tevatron. At RHIC one can measure jet-hadron correlations for rather not too high transverse momenta of the trigger photon and of the associated hadron. This is precisely the semihard region discussed here. In this case theoretical calculations would require inclusion of the fragmentation process. This can be done easily assuming an independent parton fragmentation method using fragmentation functions extracted from e^+e^- collisions. This will be the subject of the following analysis.

ACKNOWLEDGMENTS

We are indebted to Jan Rak from the PHENIX Collaboration for the discussion of recent results for photon-hadron correlations at RHIC. This work was partially supported by the grant of the Polish Ministry of Scientific Research and Information Technology No. 1 P03B 028 28.

APPENDIX

1. Matrix elements for 2 → 2 processes with initial off-shell partons

In this paper we include four $2 \to 2$ processes such as $q\bar{q} \to \gamma g$, $\bar{q}q \to \gamma g$, $gq \to \gamma q$, $qg \to \gamma q$ important at midrapidity and relatively small transverse momenta. The corresponding matrix elements for the on-shell initial partons read

$$\overline{|\mathcal{M}_{q\bar{q}\to\gamma g}|^2} = \pi\alpha_{\text{em}}\sqrt{\alpha_{1,s}\alpha_{2,s}}(16\pi)\left(\frac{8}{9}\right)\left(\frac{\hat{u}}{\hat{t}} + \frac{\hat{t}}{\hat{u}}\right),$$

$$\overline{|\mathcal{M}_{\bar{q}q\to\gamma g}|^2} = \pi\alpha_{\text{em}}\sqrt{\alpha_{1,s}\alpha_{2,s}}(16\pi)\left(\frac{8}{9}\right)\left(\frac{\hat{t}}{\hat{u}} + \frac{\hat{u}}{\hat{t}}\right),$$

$$\overline{|\mathcal{M}_{gq\to\gamma q}|^2} = \pi\alpha_{\text{em}}\sqrt{\alpha_{1,s}\alpha_{2,s}}(16\pi)\left(-\frac{1}{3}\right)\left(\frac{\hat{u}}{\hat{s}} + \frac{\hat{s}}{\hat{u}}\right),$$

$$\overline{|\mathcal{M}_{qg\to\gamma q}|^2} = \pi\alpha_{\text{em}}\sqrt{\alpha_{1,s}\alpha_{2,s}}(16\pi)\left(-\frac{1}{3}\right)\left(\frac{\hat{t}}{\hat{s}} + \frac{\hat{s}}{\hat{t}}\right).$$

The matrix elements for the off-shell initial partons were derived in Ref. [6]. To a good approximation the matrix elements for the off-shell initial partons can be also obtained by using on-shell formulas but with $\hat{s}, \hat{t}, \hat{u}$ calculated including off-shell initial kinematics. In this case $\hat{s} + \hat{t} + \hat{u} = k_1^2 + k_2^2$, where $k_1^2, k_2^2 < 0$ denote virtualities of initial partons. Our prescription can be treated as a smooth analytic continuation of the on-shell formula off mass shell. With our choice of initial parton four-momenta $k_1^2 = -k_{1,t}^2$ and $k_2^2 = -k_{2,t}^2$.

Explicit formulas for exact off-shell matrix elements were calculated and can be found in Ref. [6]. In this paper

we compare results obtained with both (approximate and exact) ways.

2. Matrix elements for $2 \to 3$ processes

In order to obtain parton-parton $\to \gamma$-jet matrix elements for the next-to-leading order one can use the following expression:

$$\frac{1}{4}\sum_{\text{spins}}\frac{1}{N_C}\sum_{\text{col}}|M|^2 = C_F 4\pi\alpha e_q^2 g_{1,s}^2 g_{2,s}^2\Big[2\Big(C_F-\frac{1}{2}N_C\Big)a_4 + N_C\frac{a_2a_7+a_3a_6}{a_9}\Big]\Big[\frac{a_1^2+a_5^2}{a_2a_3a_6a_7} + \frac{a_2^2+a_6^2}{a_1a_3a_5a_7}+\frac{a_1^3+a_7^2}{a_1a_2a_5a_6}\Big]$$

for the $\gamma(p_1)+q(p_2)\to g(k_1)+g(k_3)+q(k_2)$ process obtained in [5]. Here $C_F=4/3$, $N_C=3$,

$$g_{1,s}^2 = 4\pi\alpha_s(p_{1,t}^2) \qquad g_{2,s}^2 = 4\pi\alpha_s(p_{2,t}^2)$$

and

$$\begin{array}{llll} a_1 = p_2\cdot p_1, & a_5 = k_2\cdot p_1, & a_8 = k_3\cdot p_1, & a_{10} = k_1\cdot p_1,\\ a_2 = p_2\cdot k_1, & a_6 = k_2\cdot k_1, & a_9 = k_3\cdot k_1, & \\ a_3 = p_2\cdot k_3, & a_7 = k_2\cdot k_3, & & \\ a_4 = p_2\cdot k_2, & & & \end{array}$$

are redundant invariants. The longitudinal momentum fractions are calculated as

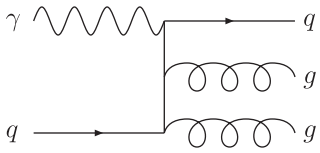

FIG. 19. Diagram of the $\gamma q \to ggq$ process.

$$x_1 = (p_{1,t}e^{y_1} + p_{2,t}e^{y_2} + p_{3,t}e^{y_3})/\sqrt{s}$$
$$x_2 = (p_{1,t}e^{-y_1} + p_{2,t}e^{-y_2} + p_{3,t}e^{-y_3})/\sqrt{s}$$

As an example the expression for matrix elements for the second diagram

$$g(p_1)+g(p_2)\to\gamma(k_1)+q(k_3)+\bar{q}(k_2)$$

in Fig. 2(b) we get from

$$\overbrace{\gamma(p_1)}+\underbrace{q(p_2)}\to\overbrace{g(k_1)}+\underbrace{g(k_3)}+q(k_2)$$

diagram (see Fig. 19) if we make the following replacement:

$$p_1\to k_1, \qquad k_1\to p_1, \qquad p_2\to k_3, \qquad k_3\to p_2,$$

thus obtaining

$$\begin{array}{llll} a_1\to a_9, & a_5\to a_6, & a_8\to a_2, & a_{10}\to a_{10},\\ a_2\to a_8, & a_6\to a_5, & a_9\to a_1, & \\ a_3\to a_3, & a_7\to a_4, & & \\ a_4\to a_7, & & & \end{array}$$

[1] S. S. Adler *et al.* (PHENIX Collaboration), Phys. Rev. Lett. **97**, 052301 (2006); Phys. Rev. C **73**, 054903 (2006); Phys. Rev. Lett. **96**, 222301 (2006); M. Oldenburg *et al.* (STAR Collaboration), Nucl. Phys. **A774**, 507 (2006).

[2] S. S. Adler *et al.* (PHENIX Collaboration), Phys. Rev. D **74**, 072002 (2006).

[3] DongJo Kim, in Proceedings of the International Workshop on High-p_t Processes at LHC, Jyväskylä, Finland, 2007 (to be published).

[4] F. A. Berends, R. Kleiss, P. De Causmaecker, R. Gastmans, and T. T. Wu, Phys. Lett. B **103**, 124 (1981).

[5] P. Aurenche, A. Baier, A. Douiri, M. Fontannaz, and D. Schiff, Nucl. Phys. **B286**, 553 (1987).

[6] A. V. Lipatov and N. P. Zotov, Phys. Rev. D **72**, 054002 (2005); J. Phys. G **34**, 219 (2007).

[7] T. Pietrycki and A. Szczurek, Phys. Rev. D **75**, 014023 (2007).

[8] C. B. Mariotto, M. B. Gay Ducati, and M. V. T. Machado, Phys. Rev. D **66**, 114013 (2002).

[9] M. Łuszczak and A. Szczurek, Phys. Lett. B **594**, 291 (2004).

[10] S. P. Baranov and M. Smizanska, Phys. Rev. D **62**, 014012 (2000).

[11] M. Łuszczak and A. Szczurek, Phys. Rev. D **73**, 054028 (2006).

[12] P. Hagler, R. Kirschner, A. Schafer, L. Szymanowski, and O. V. Teryaev, Phys. Rev. D **63**, 077501 (2001).

[13] P. Hagler, R. Kirschner, A. Schafer, L. Szymanowski, and O. V. Teryaev, Phys. Rev. Lett. **86**, 1446 (2001).

[14] J. Kwieciński and A. Szczurek, Nucl. Phys. **B680**, 164 (2004).

[15] A. V. Lipatov and N. P. Zotov, Eur. Phys. J. C **44**, 559 (2005); arXiv:hep-ph/0510043.

[16] M. Łuszczak and A. Szczurek, Eur. Phys. J. C **46**, 123 (2006).

[17] J. Kwieciński, Acta Phys. Pol. B **33**, 1809 (2002); A. Gawron and J. Kwieciński, Acta Phys. Pol. B **34**, 133 (2003); A. Gawron, J. Kwieciński, and W. Broniowski, Phys. Rev. D **68**, 054001 (2003).

[18] M. A. Kimber, A. D. Martin, and M. G. Ryskin, Phys. Rev. D **63**, 114027 (2001).

[19] J. F. Owens, Rev. Mod. Phys. **59**, 465 (1987).

[20] U. d'Alesio and F. Murgia, Phys. Rev. D **70**, 074009 (2004).

[21] M. Glück, E. Reya, and A. Vogt, Eur. Phys. J. C **5**, 461 (1998).